



Rapid chemical vapor deposition of graphene using methanol as a precursor

Imbok Lee¹ · Jungtae Nam^{1,2} · Sang Jun Park¹ · Dong Jae Bae¹ · Suklyun Hong¹ · Keun Soo Kim¹

Received: 22 April 2020 / Revised: 29 June 2020 / Accepted: 11 July 2020 / Published online: 22 July 2020
© Korean Carbon Society 2020

Abstract

In this study, graphene was rapidly grown by chemical vapor deposition using a liquid cell for supplying methanol as a carbon source of graphene. To realize the rapid growth, methanol which is carbon-contained organic solvent was used instead of methane gas, a widely used carbon source for graphene growth. The graphene grown with the growth time as a variable was transferred to a SiO₂/Si substrate with an oxide thickness of 300 nm to confirm whether it was grown with full coverage with an optical microscope. The results confirmed a full coverage in 0.5 min of growth. The Raman spectra also confirmed the G-peak position at 1585.0 cm⁻¹ and an intensity ratio of 2D/G at 2.3 or higher. Concerning electrical transport characteristics, at an induced carrier density of 1 × 10¹² cm⁻², the hole (μ_h) and electron (μ_e) mobilities were 1524 cm² V⁻¹ s⁻¹ and 1528 cm² V⁻¹ s⁻¹, respectively. Thus, our study confirmed that high-quality, large-area graphene can be grown within 0.5 min.

Keywords Graphene · Films · Chemical vapor deposition · Optical properties · Electronic transport

1 Introduction

At the first derivation of the characteristics of graphene by separation from graphite [1], its remarkable electrical [2–4], thermal [5], optical [6, 7], and mechanical properties [8, 9] were investigated globally. In addition, many efforts have been made to industrialize high-quality graphene for using its superb properties [10–12]. The chemical vapor deposition (CVD) method is one of the potential methods for mass production of graphene [13–17], and it is easy to fabricate large-scale graphene for transparent electrodes [13, 18, 19], solar cells [20, 21], and in other applications [15, 22]. In addition

to experimental studies, theoretical studies involving DFT simulated the phenomenon occurring at the atomic level during the growth of graphene or the formation of doped graphene in CVD [23, 24]. It has the advantage of being able to understand the growth of graphene with various characteristics by perturbation of growth conditions. According to Liu [25], to achieve industrialization, graphene's thickness uniformity, lateral size, low defect density, yield, and low cost are required. In the case of CVD graphene, there are two challenges. One is the yield, and the other is the cost. Concerning cost, the constant consumption of catalytic metal, which disappears in the transfer process and high-power consumption by heating the catalytic metal to almost 1000 °C to the synthesis of high-quality graphene, must be solved. The consumption of catalytic metal can be solved by adopting the electro-delamination transfer process in which catalytic metal and graphene are separated without any damage to the catalytic metal [26–28]. Furthermore, batch-to-batch (B2B) or roll-to-roll (R2R) structure represent one step further to the mass production [19, 29]. In the case of the consumption of power, there are two options. One is to lower the growth temperature [30], and the other is to reduce the synthesis time [29].

To improve the productivity of CVD graphene, we used methanol, which has a chemical formula similar to that of methane gas commonly used in chemical vapor deposition of

Imbok Lee and Jungtae Nam contributed equally to this paper.

Electronic supplementary material The online version of this article (<https://doi.org/10.1007/s42823-020-00166-6>) contains supplementary material, which is available to authorized users.

✉ Keun Soo Kim
kskim2676@sejong.ac.kr

¹ Department of Physics and GRI-TPC International Research Center, Sejong University, Seoul 05006, Republic of Korea

² Carbon Convergence Materials Research Center, Institute of Advanced Composites Materials, Korea Institute of Science and Technology, Wanju-gun 55324, Republic of Korea

graphene, but a different phase, which is an organic solvent as a precursor. As a result, we succeeded in synthesizing the graphene growth rate over ten times faster than that of methane gas [31, 32].

2 Experimental

2.1 Graphene growth

Graphene was grown via thermal–chemical vapor deposition (T-CVD) using a copper foil as a catalytic substrate. 18- μm -thick single-side-polished copper foil was selected for this experimental. As shown in Fig. 1b, graphene growth was segmented into four sections. First, T-CVD was heated to 1000 °C for 30 min with 100 sccm argon as a carrier gas. Before supplying the carbon source for growing graphene, hydrogen gas was flowed at 50 sccm for 10 min to activate the copper foil surface by eliminating the copper oxide and other contaminants. The graphene growth condition is changed by controlling the growth time. Methanol was supplied for 0.5 min, 1 min, and 5 min using the liquid cell and the gradient of partial pressure between the liquid cell and the main chamber, as shown in Fig. 1a. During this process, the vacuum condition in the T-CVD chamber was maintained at 140 mTorr, which implies that the same amount of methanol was supplied with the methane supply case [31]. The catalytic copper foil was rapidly cooled by removing

the heating element after finishing the graphene growth to prevent the dewing of additional carbon.

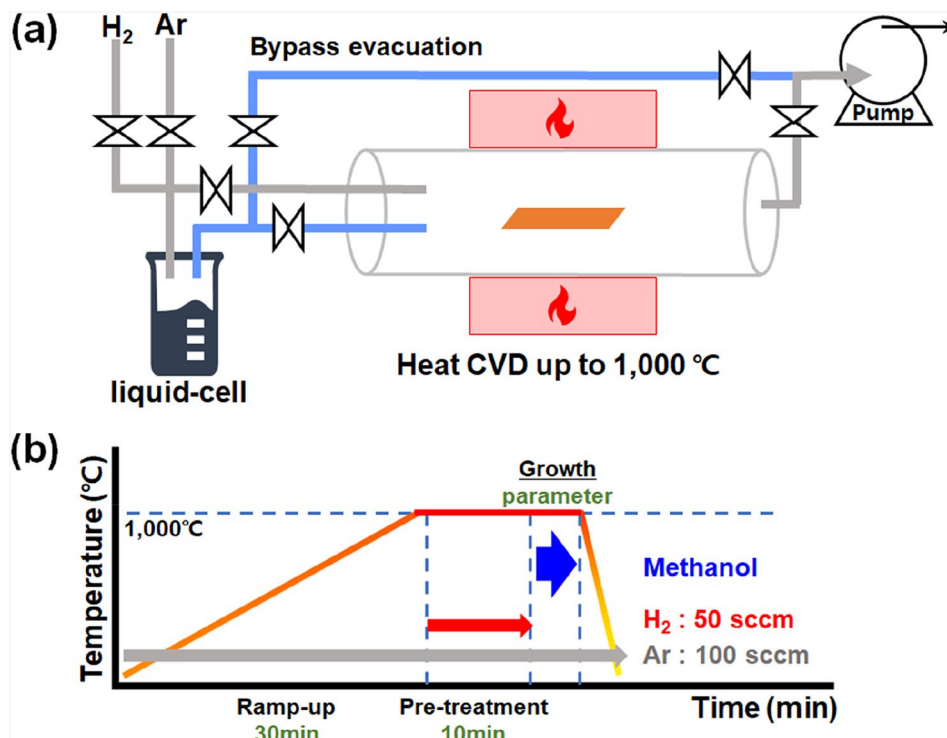
2.2 Graphene transfer

To transfer graphene onto the SiO_2/Si substrate, graphene/Cu foil after backside etching was coated by poly(methyl methacrylate) 950 K C4 from MicroChem using a spin-coating technique. The PMMA/graphene/Cu foil was placed in 0.15 M ammonium persulfate (APS) solution to etch the Cu foil from the sample. The separated PMMA/graphene film was moved onto the SiO_2/Si substrate after rinsing several times on DI-water to prevent contamination of etched copper and residual etchant. Finally, the PMMA on the graphene was eliminated by acetone.

2.3 Characterization

To determine the role of growth time, graphene was characterized using an optical microscope. Through the optical microscope image, the coverage of graphene was investigated. Raman spectra were measured at ten points for each sample using a Renishaw inVia Raman spectroscope with a 514 nm laser source. The electrical properties of graphene were determined via a graphene-field effect transistor (G-FET). The source–drain channel of the G-FET was 3.5 μm \times 3.0 μm , and a back-gate was chosen with a 300-nm SiO_2 gate oxide by electron beam lithography. The electron and hole mobilities of graphene depending on the growth

Fig. 1 Schematic illustration of T-CVD setup and conditions for graphene growth using methanol. **a** Scheme of T-CVD with gas supply using a liquid cell, **b** temperature profile and supplying gas as a function of time



time were calculated from the G-FET's operating current response of the gate voltage change measured using Keithley 236 and 237 source-measure units in the vacuum probe station below 10^{-5} Torr.

3 Results and discussion

First, to confirm the growth state of graphene, graphene transferred to a 300 nm SiO_2/Si substrate, which is the easiest to optically distinguish graphene, was confirmed using an optical microscope [33]. Figure 2a shows the graphene grown on the catalytic copper foil before transfer and Fig. 2b the transferred graphene coverage on the SiO_2/Si substrate. The minimum time required for full-covered graphene growth was confirmed by the transferred image in Fig. 2a, as graphene was synthesized on the entire surface of the substrate within 0.5 min of the growth time.

The quality of the graphene samples according to the growth time was evaluated by measuring the position and shape of the G and 2D peaks using Raman spectroscopy. Figure 3c shows representative Raman spectra, which are normalized by the G peak intensity according to the growth time of the graphene grown by methanol. All graphene samples had a distinctive G-peak at approximately 1584 cm^{-1} and a 2D peak at approximately 2680 cm^{-1} , confirming that typical CVD graphene grew well [34, 35].

To further evaluate the quality of the graphene samples according to the growth time, a closer analysis of the Raman spectra was performed by Lorentz fitting of each peak. As shown in Fig. 3a and b, the G-peak positions were 1585.0 cm^{-1} , 1584.6 cm^{-1} , and 1586.4 cm^{-1} at growth times of 0.5 min, 1 min, and 5 min, respectively. Considering that the G peak position of CVD graphene appeared at approximately 1583 cm^{-1} [34–36], the disturbance occurred in phonon vibration due to oxygen- or hydroxyl-related components present in methanol used as a carbon source, causing blue-shift assumed to have happened. This result is in line with the electrical transport result, which will be described later.

As shown in Fig. 3a and b, the 2D peak positions of each graphene were 2679.6 cm^{-1} , 2677.6 cm^{-1} , and 2681.6 cm^{-1} at 0.5 min, 1 min, and 5 min, respectively. As shown in Fig. 3b and d, the value of the full-width at half-maximum (FWHM) of the 2D peaks [37, 38] is 34.1, 33.9, and 34.0, around 2677 cm^{-1} of the CVD graphene in a preliminary study grown with methane [31]. It was confirmed that graphene was well synthesized with methanol as a source by having a value similar to that of the 2D peak position near 2700 cm^{-1} and the FWHM value of approximately 31. The intensity of 2D/G ($I_{2D/G}$) according to the growth time was 2.3 at 0.5 min and 2.2 at 1 min, which was higher than 2.0; however, it was shown at 1.7 at 5 min. As the growth time was extended to the methanol

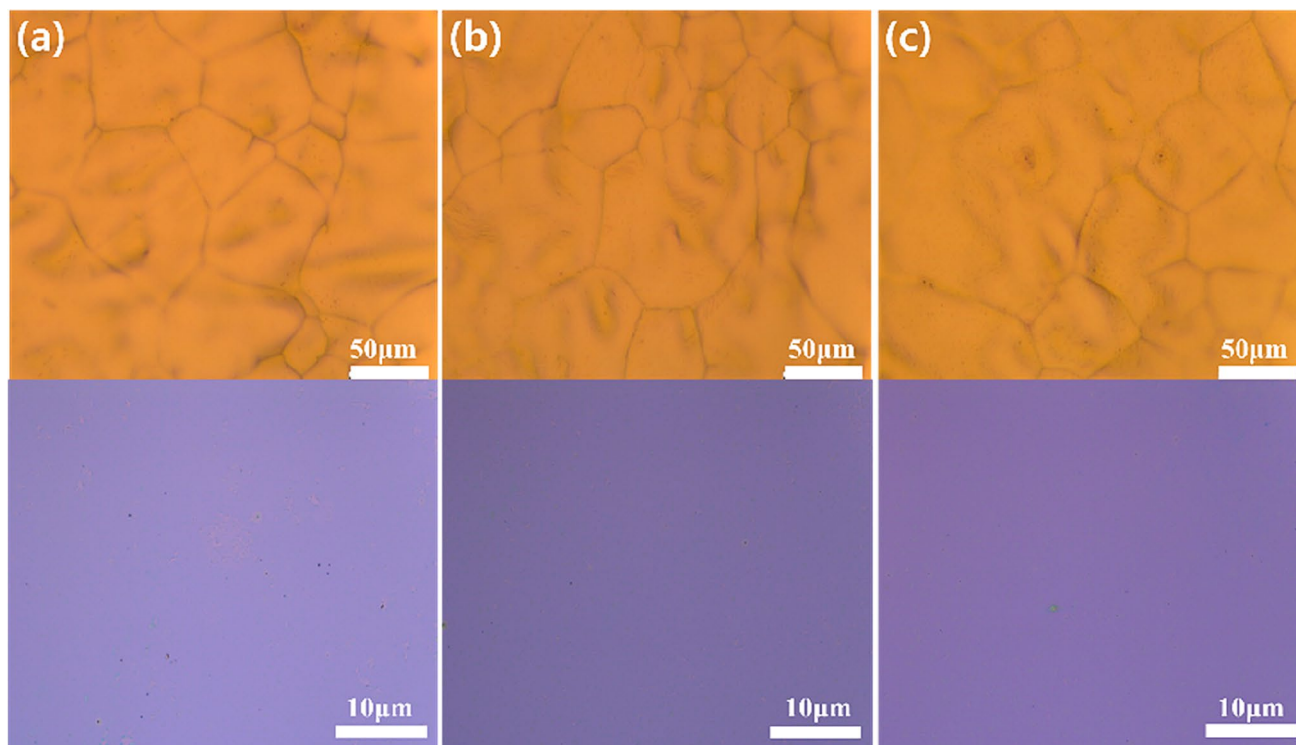


Fig. 2 Optical microscopic images of as-grown and transferred graphene. The growth times of **a–c** are 0.5 min, 1 min, and 5 min, respectively

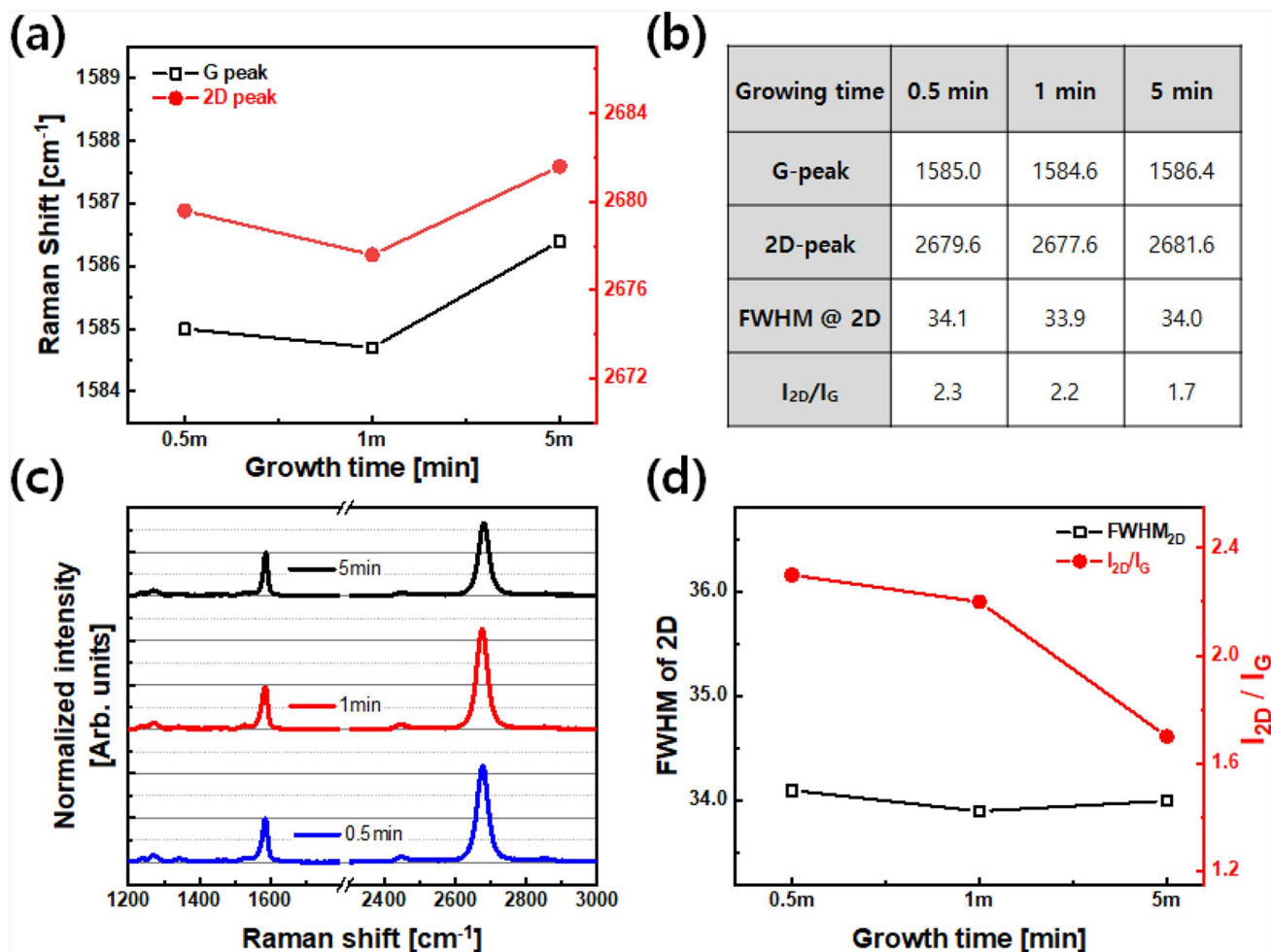


Fig. 3 Raman spectra of graphene depend on the growth time. **a** G-peak (left Y-axis) and 2D-peak (right Y-axis) position variance with increasing growth time. **b** Summary of main peak positions for each growth time of 0.5 min, 1 min, and 5 min. **c** Typical Raman

spectra of 0.5 min, 1 min, and 5 min growth graphene. Whole peaks are normalized by each G-peak intensity. **d** FWHM of 2D-peak (left Y-axis) and intensity ratio of 2D/G (right Y-axis)

supply, the growth of monolayered graphene reflected in I_{2D/G} slightly decreased.

These results can be confirmed by evaluating the electrical transport characteristics of the graphene field-effect transistor (G-FET) made of graphene ribbon (3.5 μm × 3.0 μm) as a channel [4, 39]. Figure 4a shows the back-gated G-FET for electrical transport measurements. It was measured by source-drain electrodes at both the right and left ends, and heavily P-doped Si with a gate insulator (300 nm SiO₂) was used as the gate electrode. Figure 4b represents a graph of the current between the source and drain electrodes according to the gate voltage of the G-FET made of graphene according to each growth time. Because of the hydroxyl in ethanol, all graphene exhibited P-doped properties, and the slope of the current over voltage had a similar slope in graphene grown at 0.5 min and 1 min but tended to decrease rapidly in samples grown at 5 min. More specifically, it was

confirmed that 0.5 min and 1 min grown graphene materials have a high current density and Dirac points (V_{Dirac}) of 53.5 V and 79.5 V, respectively [39]

Meanwhile, graphene grown for 5 min had a Dirac point of 45 V. The carrier mobility of each sample was calculated using Eq. (1) according to the Drude model from the measured source-drain current (channel current) as a function of gate voltage.

$$\mu = \frac{1}{n \cdot q \cdot \rho} = \frac{1}{|V_G - V_D| \cdot C_{ox} \cdot q \cdot (R_{ch} \cdot \frac{W}{L})} \quad (1)$$

In Eq. (1), 11.5102 nF/cm² was applied to C_{ox} as a capacitance of 300 nm SiO₂.

When the induced carrier concentration was 1×10^{12} cm⁻², the graphene grown for 0.5 min was 1528 cm² V⁻¹ s⁻¹ for electron mobility (μ_e), and

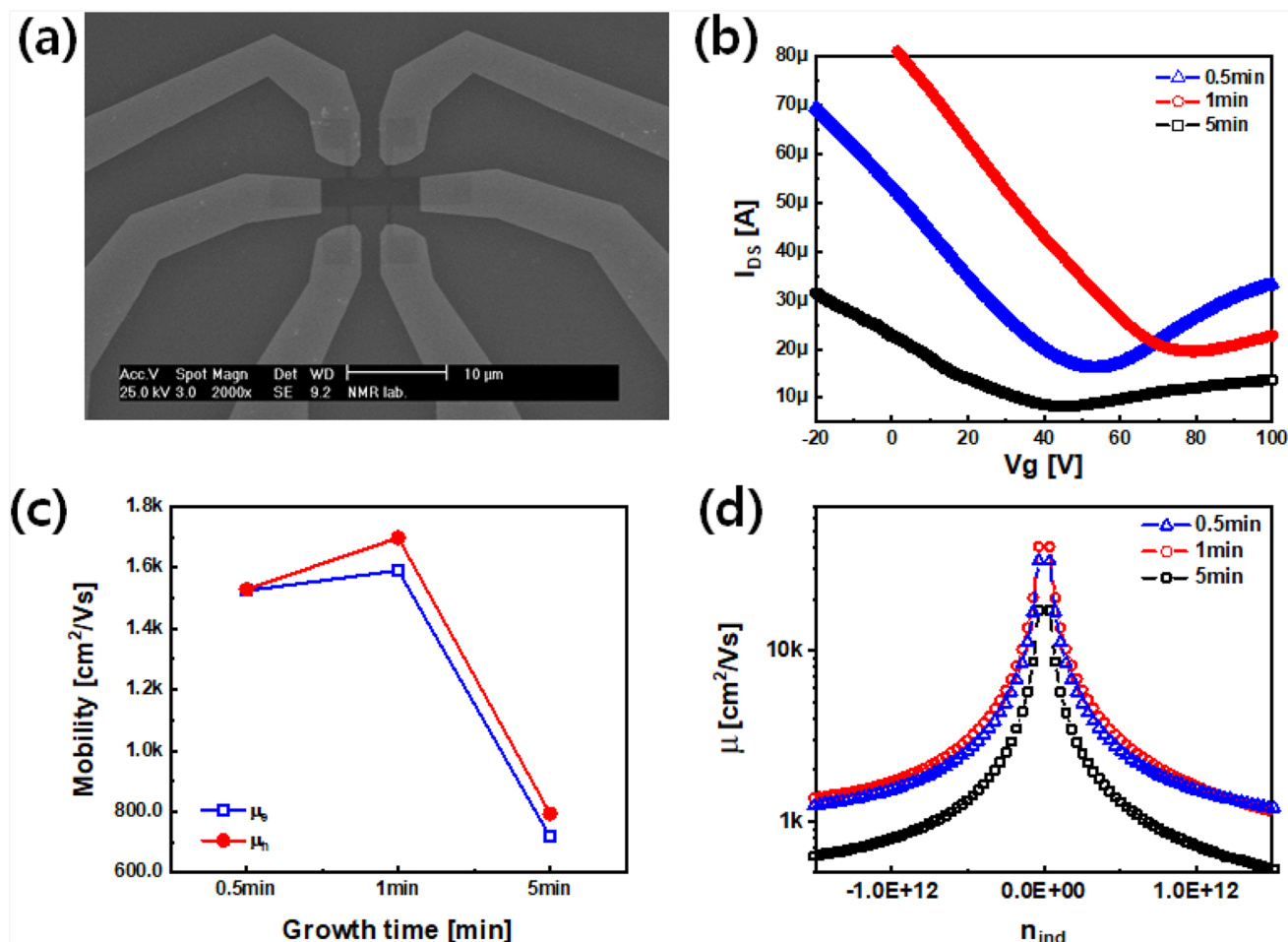


Fig. 4 G-FET image and characteristics of electrical properties. **a** SEM image of the fabricated G-FET structure, **b** source–drain current of the G-FET as a function of gate voltage at V_{ds} of 50 mV, **c**

mobility of electron and hole in G-FET at induced carrier density of $n_{ind} = 1 \times 10^{12} \text{ cm}^{-2}$, and **d** mobility of the G-FET depending on the induced carrier density

1524 $\text{cm}^2 \text{ V}^{-1} \text{ s}^{-1}$ for hole mobility (μ_h), 1 min growth graphene was measured to be 1697 and 1590 $\text{cm}^2 \text{ V}^{-1} \text{ s}^{-1}$, respectively [3, 40, 41]. In the 5 min growth of graphene, μ_e and μ_h were measured as 794 and 718 $\text{cm}^2 \text{ V}^{-1} \text{ s}^{-1}$, respectively. As confirmed in the Raman spectra, to decrease $I_{2D/G}$ as the growth time was extended, the carrier mobilities were lowered by extending the growth time due to the relatively increased defect site as the growth time increased. The 0.5 min and 1 min growth graphene materials have a similar level of carrier mobility; thus, it was confirmed that the quality of the graphene grown at that time was similarly grown at high quality, as shown as Raman spectra. Electrical transport characteristics were measured at room temperature after heat treatment at approximately 180 °C for 5 h in a vacuum to eliminate the influence of moisture and oxygen from the graphene, as much as possible. The grown graphene was hole-doped with V_{Dirac} of 53.5 V, 79.5 V, and 45 V.

4 Conclusion

In this study, graphene was grown using the CVD method. Synthesis of large-area graphene was rapidly achieved within 0.5 min of growth time using hydroxyl-bonded methanol instead of methane, which is commonly used in CVD graphene growth. Raman spectrum analysis was conducted, and it revealed that similar high-quality graphene was formed through comparison with graphene grown for 10 min with methane having a G peak of approximately 1585 cm^{-1} and intensity of 2D/G of 2.3 or more. The characteristics of graphene, according to the growth time, were confirmed by the relative comparison between the G, 2D, and D-peaks in the Raman spectra. Through the growth of graphene by the methanol precursor, within 1 min of growth time under conditions identical to those of pristine graphene by methane, which has the same carbon

precursor partial pressure, the same number of carbon atoms supplied on the catalytic substrate was enough. The electrical transport characteristics of graphene confirmed that 1 min is enough growth time. Positive values of Dirac points were confirmed for all graphene growth times; at 0.5, 1, and 5 min, they were $V_{\text{Dirac}} = 53.5$ V, 79.5 V, and 45 V, respectively. Based on the induced carrier concentration of $1 \times 10^{12} \text{ cm}^{-2}$, graphene grown for 1 min using a methanol precursor has a hole and electron mobility comparable to that of pristine graphene by methane, which was shown to be over $1500 \text{ cm}^2 \text{ V}^{-1} \text{ s}^{-1}$ in hole and electron mobility. It is expected that graphene grown by methanol can be used as a mass production method for graphene, which has a throughput ten times higher than that of graphene by methane. It can also be used in high-performance electronic devices based on its p-type characteristics, which can be adopted in the field of diodes, BJT (bipolar junction transistor), CMOS (Complementary metal–oxide–semiconductor), and solder cell electrodes.

Acknowledgements This research was supported by Korea Electric Power Corporation (Grant Number: R18XA06-34) and the Global Research and Development Center Program (Grant Number: 2018K1A4A3A01064272) of the NRF funded by the Ministry of Science and ICT.

Compliance with ethical standards

Conflict of interest The authors declare that they have no conflict of interest.

References

- Novoselov KS (2004) Electric field effect in atomically thin carbon films. *Science* 306:666–669. <https://doi.org/10.1126/science.1102896>
- Tombros N, Jozsa C, Popinciuc M et al (2007) Electronic spin transport and spin precession in single graphene layers at room temperature. *Nature* 448:571–574. <https://doi.org/10.1038/nature04235>
- Chen J-H, Jang C, Xiao S et al (2008) Intrinsic and extrinsic performance limits of graphene devices on SiO_2 . *Nat Nanotechnol* 3:206–209. <https://doi.org/10.1038/nnano.2008.58>
- Zhang Y, Tan Y-W, Stormer HL, Kim P (2005) Experimental observation of the quantum Hall effect and Berry's phase in graphene. *Nature* 438:201–204. <https://doi.org/10.1038/nature04235>
- Balandin AA, Ghosh S, Bao W et al (2008) Superior thermal conductivity of single-layer graphene. *Nano Lett* 8:902–907. <https://doi.org/10.1021/nl0731872>
- Mak KF, Sfeir MY, Wu Y et al (2008) Measurement of the optical conductivity of graphene. *Phys Rev Lett* 101:196405. <https://doi.org/10.1103/PhysRevLett.101.196405>
- Nair RR, Blake P, Grigorenko AN et al (2008) Fine structure constant defines visual transparency of graphene. *Science* 320:1308–1308. <https://doi.org/10.1126/science.1156965>
- Booth TJ, Blake P, Nair RR et al (2008) Macroscopic graphene membranes and their extraordinary stiffness. *Nano Lett* 8:2442–2446. <https://doi.org/10.1021/nl801412y>
- Lee C, Wei X, Kysar JW, Hone J (2008) Measurement of the elastic properties and intrinsic strength of monolayer graphene. *Science* 321:385–388. <https://doi.org/10.1126/science.1157996>
- Bonaccorso F, Sun Z, Hasan T, Ferrari AC (2010) Graphene photonics and optoelectronics. *Nat Photonics* 4:611–622. <https://doi.org/10.1038/nphoton.2010.186>
- Wang Y, Tong SW, Xu XF et al (2011) Interface engineering of layer-by-layer stacked graphene anodes for high-performance organic solar cells. *Adv Mater* 23:1514–1518. <https://doi.org/10.1002/adma.201003673>
- Cohen-Tanugi D, Grossman JC (2012) Water desalination across nanoporous graphene. *Nano Lett* 12:3602–3608. <https://doi.org/10.1021/nl3012853>
- Kim KS, Zhao Y, Jang H et al (2009) Large-scale pattern growth of graphene films for stretchable transparent electrodes. *Nature* 457:706
- Li X, Cai W, An J et al (2009) Large-area synthesis of high-quality and uniform graphene films on copper foils. *Science* 324:1312–1314. <https://doi.org/10.1126/science.1171245>
- Ito K, Katagiri M, Sakai T, Awano Y (2013) Electrical resistivity measurements of layer number determined multilayer graphene wiring for future large scale integrated circuit interconnects. *Jpn J Appl Phys*. <https://doi.org/10.7567/JJAP.52.06GD08>
- Reina A, Jia X, Ho J et al (2009) Large area, few-layer graphene films on arbitrary substrates by chemical vapor deposition. *Nano Lett* 9:30–35. <https://doi.org/10.1021/nl801827v>
- Cao H, Yu Q, Colby R et al (2010) Large-scale graphitic thin films synthesized on Ni and transferred to insulators: structural and electronic properties. *J Appl Phys* 107:044310. <https://doi.org/10.1063/1.3309018>
- Gomez De Arco L, Zhang Y, Schlenker CW et al (2010) Continuous, highly flexible, and transparent graphene films by chemical vapor deposition for organic photovoltaics. *ACS Nano* 4:2865–2873. <https://doi.org/10.1021/nn901587x>
- Kobayashi T, Bando M, Kimura N et al (2013) Production of a 100-m-long high-quality graphene transparent conductive film by roll-to-roll chemical vapor deposition and transfer process. *Appl Phys Lett* 102:023112. <https://doi.org/10.1063/1.4776707>
- Choe M, Lee BH, Jo G et al (2010) Efficient bulk-heterojunction photovoltaic cells with transparent multi-layer graphene electrodes. *Org Electron* 11:1864–1869. <https://doi.org/10.1016/j.orgel.2010.08.018>
- Jo G, Na S-I, Oh S-H et al (2010) Tuning of a graphene-electrode work function to enhance the efficiency of organic bulk heterojunction photovoltaic cells with an inverted structure. *Appl Phys Lett* 97:213301. <https://doi.org/10.1063/1.3514551>
- Wang M, Jang SK, Jang W-J et al (2013) A platform for large-scale graphene electronics—CVD growth of single-layer graphene on CVD-grown hexagonal boron nitride. *Adv Mater* 25:2746–2752. <https://doi.org/10.1002/adma.201204904>
- Goyenola C, Stafström S, Schmidt S et al (2014) Carbon fluoride, CF_x : structural diversity as predicted by first principles. *J Phys Chem C* 118:6514–6521. <https://doi.org/10.1021/jp500653c>
- Refaely-Abramson S, Baer R, Kronik L (2011) Fundamental and excitation gaps in molecules of relevance for organic photovoltaics from an optimally tuned range-separated hybrid functional. *Phys Rev B* 84:075144. <https://doi.org/10.1103/PhysRevB.84.075144>
- Lin L, Peng H, Liu Z (2019) Synthesis challenges for graphene industry. *Nat Mater* 18:520–524. <https://doi.org/10.1038/s41563-019-0341-4>
- Cherian CT, Giustiniano F, Martin-Fernandez I et al (2015) 'Bubble-Free' electrochemical delamination of CVD graphene films. *Small* 11:189–194. <https://doi.org/10.1002/smll.201402024>
- Nam J, Lee I, Lee DY et al (2020) Abnormal grain growth for single-crystal Cu substrate and chemical vapor deposition of

- graphene on it. *J Korean Phys Soc* 76:923–927. <https://doi.org/10.3938/jkps.76.923>
28. Nam J, Kim D-C, Yun H et al (2017) Chemical vapor deposition of graphene on platinum: growth and substrate interaction. *Carbon* 111:733–740. <https://doi.org/10.1016/j.carbon.2016.10.048>
 29. Lee I, Bae DJ, Lee WK et al (2019) Rapid synthesis of graphene by chemical vapor deposition using liquefied petroleum gas as precursor. *Carbon* 145:462–469. <https://doi.org/10.1016/j.carbon.2019.01.004>
 30. Yamada T, Kim J, Ishihara M, Hasegawa M (2013) Low-temperature graphene synthesis using microwave plasma CVD. *J Phys Appl Phys* 46:063001. <https://doi.org/10.1088/0022-3727/46/6/063001>
 31. Choi DS, Kim KS, Kim H et al (2014) Effect of cooling condition on chemical vapor deposition synthesis of graphene on copper catalyst. *ACS Appl Mater Interfaces* 6:19574–19578. <https://doi.org/10.1021/am503698h>
 32. Park SJ, Lee I, Bae DJ et al (2015) Controlling the properties of graphene using CVD method: pristine and N-doped graphene. *KEPCO J Electr Power Energy* 1:169–174. <https://doi.org/10.18770/KEPCO.2015.01.01.169>
 33. Blake P, Hill EW, Castro Neto AH et al (2007) Making graphene visible. *Appl Phys Lett* 91:063124. <https://doi.org/10.1063/1.2768624>
 34. Ferrari AC (2007) Raman spectroscopy of graphene and graphite: Disorder, electron–phonon coupling, doping and nonadiabatic effects. *Solid State Commun* 143:47–57. <https://doi.org/10.1016/j.ssc.2007.03.052>
 35. Malard LM, Pimenta MA, Dresselhaus G, Dresselhaus MS (2009) Raman spectroscopy in graphene. *Phys Rep* 473:51–87. <https://doi.org/10.1016/j.physrep.2009.02.003>
 36. Ferrari AC, Basko DM (2013) Raman spectroscopy as a versatile tool for studying the properties of graphene. *Nat Nanotechnol* 8:235–246. <https://doi.org/10.1038/nnano.2013.46>
 37. Ferrari AC, Meyer JC, Scardaci V et al (2006) Raman spectrum of graphene and graphene layers. *Phys Rev Lett* 97:187401. <https://doi.org/10.1103/PhysRevLett.97.187401>
 38. Park JS, Reina A, Saito R et al (2009) G' band Raman spectra of single, double and triple layer graphene. *Carbon* 47:1303–1310. <https://doi.org/10.1016/j.carbon.2009.01.009>
 39. Schwierz F (2010) Graphene transistors. *Nat Nanotechnol* 5:487–496. <https://doi.org/10.1038/nnano.2010.89>
 40. Kim S, Nah J, Jo I et al (2009) Realization of a high mobility dual-gated graphene field-effect transistor with Al₂O₃ dielectric. *Appl Phys Lett* 94:062107. <https://doi.org/10.1063/1.3077021>
 41. Venugopal A, Chan J, Li X et al (2011) Effective mobility of single-layer graphene transistors as a function of channel dimensions. *J Appl Phys* 109:104511. <https://doi.org/10.1063/1.3592338>

Publisher's Note Springer Nature remains neutral with regard to jurisdictional claims in published maps and institutional affiliations.